Analysis of vertical projectile penetration in granular soils

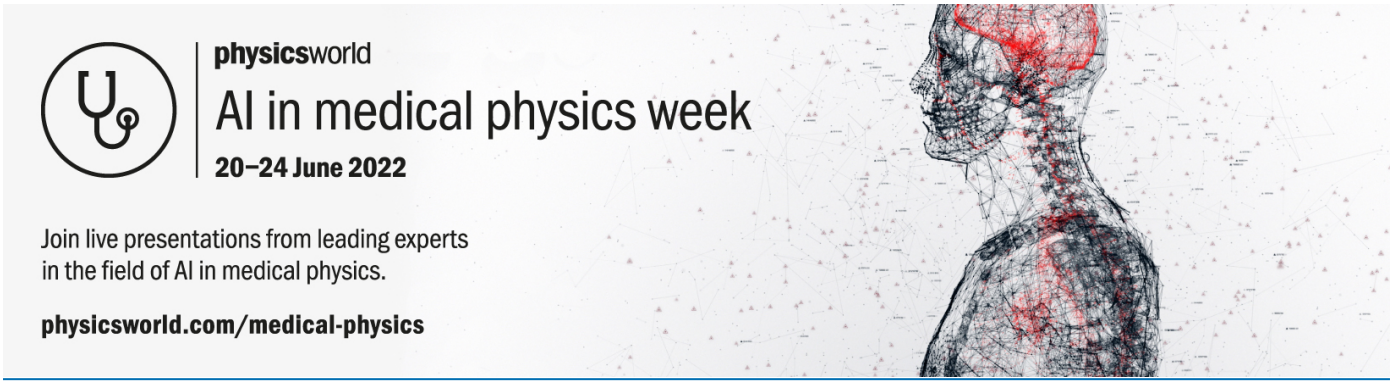

J. Phys. D: Appl. Phys. **29** (1996) 905–916. Printed in the UK

Analysis of vertical projectile penetration in granular soils

Yu Boguslavskii, S Drabkin and A Salman

Polytechnic University, Brooklyn, New York 11201, USA

Received 25 August 1995, in final form 14 November 1995

Abstract. A model of vertical dynamic penetration of projectiles in granular soils was developed based on known experiments and the theory of dimensions. The depth of penetration is derived as a function of initial velocity and material properties. Velocity and acceleration are obtained as functions of time and depth of penetration. Under certain conditions two acceleration peaks are observed, an initial one due to dynamic and a second one due to static characteristics of penetration. Static properties of soils are derived using dynamic measurements. Numerical examples are provided. Theoretical and experimental results coincide reasonably well.

Symbols

C	dimensionless constant depending on the shape of the projectile
C_1	constant depending on the shape of the projectile
F	net resistant force
F_1	dissipative component of resistance force
F_2	dynamic component of resistance force
F_3	static component of resistance force
g	acceleration due to gravity
H	depth of penetration
H_e	depth of projectile penetration for maximum $\dot{H}$
H_m	maximum depth of projectile penetration
$\dot{H}$	velocity of the projectile in granular media
$\ddot{H}$	acceleration of the projectile in granular media
m	mass of the projectile
$\ddot{H}_m$	maximum deceleration of the projectile
P	weight of the projectile
s	cross sectional area of the projectile in the direction of penetration
v_0	initial velocity of penetration
γ_0	resistance coefficient
μ	shear modulus
ϱ	density of granular media

1. Introduction

Soil penetration by projectiles has interested many generations of researchers. Historically, studies in projectile penetrations were initiated according to military needs more than two centuries ago (Euler 1745, Robins 1742). More recent studies by Allen *et al* (1957), Rachmatullin *et al* (1964), Thompson (1975), True (1976), Sogomonyan (1974) and Zukas *et al* (1982) have focused on the impact and subsequent penetration of instrumented projectiles used for soil investigation.

Experimental studies on the dynamics of soil penetration by low-velocity projectiles stimulated the development of theoretical modelling of the dynamic phenomena of impact penetration in solids (Zukas *et al* 1982) and in soils (Sogomonyan 1974). These theories were mostly based on dynamic plasticity and dynamic wave propagation and did not adequately characterize the extremely complex process of vertical penetration in granular soils.

The need still exists for remote soil exploration. Current experimental studies have concentrated on assessment of the influence of projectile shape on depth of penetration (Forrestal *et al* 1986, 1991), or fitting of results to existing theoretical models (Taylor *et al* 1991, Hearst and Lynch 1994). Such an approach avoids analysis of the physical properties of penetration phenomena.

This paper develops a comprehensive model of projectile penetration at sub-sonic velocities in granular media. Hence clear physical understanding of the processes governing the projectile's deceleration was acquired. Comparison of theoretical and experimental results allowed us to solve the inverse problem of dynamic penetration and to determine the properties of penetrated non-cohesive granular media.

2. Experimental studies of penetration phenomena in uniform sand media

Among available sources mentioned in the introduction, the most comprehensive experimental study of penetration phenomena was performed by Thompson (1975). He investigated vertical penetration of a projectile into homogeneous sand (figure 1(*a*)).

The initial impact velocity of penetration v_0 varied in the range 0.0–46 m s^{-1}. In the experiments with initial velocity of 0.0 m s^{-1}, the projectile was accelerated by

0022-3727/96/030905+12$19.50

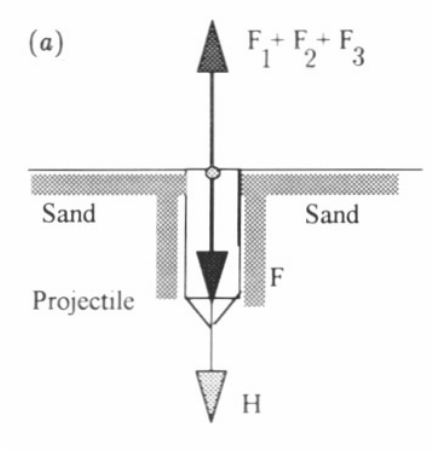

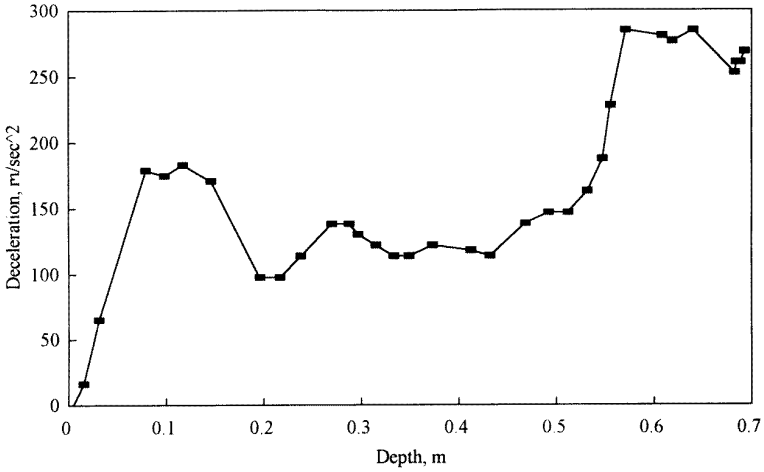

Figure 1. (*a*) Forces acting on a penetrating projectile. (*b*) Penetrometer deceleration for $v_0 = 16$ m s^{-1} in sand of medium density in a vacuum test.

gravitation from rest when it was released with its point just in contact with the surface of the bed. To achieve higher velocities, Thompson used a compressed gas gun. The projectile consisted of a 70.5 mm long cone nose attached to a 400 mm long, 38 mm diameter afterbody. The weight of the penetrometer was 2.715 kg. Inside the nose there was installed an accelerometer, that was used to assess the deceleration of the penetrometer with time and depth.

The target was sand with 10% of grain diameters smaller than 0.27 mm, 50% of diameters smaller than 0.4 mm and 90% of diameters less than 1 mm. Such sand is usually considered to be homogeneous. Three different densities of sand were tested. The minimum density was 1451 kg m^{-3}; the medium and maximum densities were 1593 and 1700 kg m^{-3}, respectively. The targets were penetrated at atmospheric pressure (atmospheric tests) and in a vacuum chamber (vacuum tests).

Thompson evaluated the static resistance of tested sands using cone penetration tests. A hydraulic piston maintained the rate of penetration at 0.002 m s^{-1}. The load cell measured the total force transmitted by the piston both to the penetrometer cone and to the penetrometer afterbody. This afterbody was of the same diameter as the penetrometer and had a polished surface similar to that of the penetrometer. It prevented the sand from collapsing onto the rear of the penetrometer after the penetrometer had been submerged in the sand deposit. Skin friction was assessed using a separate load cell.

3. The theory of penetration

The general relation of the dynamic penetration problem of a rigid penetrator in a yielding target may be written in accordance with Newton's second law as follows:

$$m\ddot{H}(t) = -F + P \tag{1}$$

where m, $\ddot{H}(t)$ and $H(t)$ are the projectile's mass, acceleration and depth of penetration, F is the net resistant force, $P = mg$ is the weight of the projectile with g being the acceleration due to gravity. The depth H is measured positive in the downward direction; the origin of H is at the surface of the bed of granular soil (figure 1(*a*)). The net resistance F may be expressed as

$$F = F_1 + F_2 + F_3 \tag{2}$$

where F_1, F_2 and F_3 are respectively the dissipative, dynamic and static components of the resistance force. This

force F should be defined in such a manner that it could be used for evaluation of experimental results.

The dissipative component F_1 depends on losses due to viscosity and wave generation in the granular media. However, the results of experiments (Jaeger and Nagel 1992) have shown that viscosity may be neglected in granular media. At sub-sonic velocities in media, the resistance F_1 associated with compressibility or wave-generation may be neglected too.

In a projectile–soil system, the parameters important for evaluation of F_2 are the projectile's velocity $\dot{H}(t)$, the cross sectional area in the direction of penetration s and the soil's density ϱ. Assuming F_2 to be independent of H and using the general dimensional theory (Sedov 1959), F_2 may be expressed as

$$F_2 = C\varrho s(\dot{H}(t))^2$$

because only this combination of $\dot{H}(t)$, s and ϱ has the dimensions of force. Here C is a dimensionless constant depending only on the shape of a projectile. The static component of resistance force, F_3, is a function of $H(t)$ for vertical penetration and depends on the same constant factors as does F_2.

The experimental results (figure 1(b)) show non-monotonic correlations between the variation of projectile deceleration with time and the depth of penetration. Therefore, F may be considered to be a composite function of variables $\dot{H}^2$ and H. Though the function $F = F(\dot{H}^2, H)$ is unknown, it may be expressed as a Maclaurin series expansion:

$$\begin{aligned} F = {} & F(0,0) + \frac{\partial F(0,0)}{\partial(\dot{H})^2}\dot{H}^2 + \frac{\partial F(0,0)}{\partial H}H \\ & + \frac{1}{2}\left(\frac{\partial^2 F(0,0)}{\partial(\dot{H}^2)^2}\dot{H}^4 + 2\frac{\partial^2 F(0,0)}{\partial H\partial(\dot{H}^2)}H\dot{H}^2 \right. \\ & \left. + \frac{\partial^2 F(0,0)}{\partial H^2}H^2\right) + \frac{1}{3!}\left(\frac{\partial^3 F(0,0)}{\partial(\dot{H}^2)^3}\dot{H}^6 \right. \\ & + 3\frac{\partial^3 F(0,0)}{\partial(\dot{H}^2)^2\partial H}(\dot{H}^2)^2 H + 3\frac{\partial^3 F(0,0)}{\partial(\dot{H}^2)\partial H^2}\dot{H}^2 H^2 \\ & \left. + \frac{\partial^3 F(0,0)}{\partial H^3}H^3\right) + \cdots . \end{aligned} \tag{3}$$

This equation is true for such H and $\dot{H}^2$ that the remainder after n terms converges to zero when the number of terms increases (Korn and Korn 1968). The series is a monotonically decreasing one. The terms with $\dot{H}^4$, $H^2\dot{H}^2$, H^4 and other higher order terms are considered to be small. Comparison with experiments will show the validity of this assumption. The remaining terms of (3) are substituted into equation (1). Were one to keep more terms in (1), its analysis would become very difficult. After dividing equation (1) by m, it may be expressed as

$$\ddot{H} = -\beta\dot{H}^2 - \gamma_0(1 + \epsilon\dot{H}^2)H - \gamma_1 H^2 - \gamma_2 H^3 + \delta \tag{4}$$

where

$$\begin{aligned} \delta &= g - \frac{F(0,0)}{m} \qquad \beta = \frac{1}{m}\frac{\partial F(0,0)}{\partial(\dot{H}^2)} = \frac{C\varrho s}{m} \\ \gamma_0 &= \frac{1}{m}\frac{\partial F(0,0)}{\partial H} \qquad \gamma_1 = \frac{1}{2m}\frac{\partial^2 F(0,0)}{\partial H^2} \\ \epsilon &= \frac{1}{m\gamma_0}\frac{\partial^2 F(0,0)}{\partial H\partial(\dot{H}^2)} \qquad \gamma_2 = \frac{1}{6m}\frac{\partial^3 F(0,0)}{\partial H^3}. \end{aligned} \tag{4'}$$

From physical considerations and dimensional analysis (Sedov 1959), γ_0, γ_1 and γ_2 from equation (4′) are

$$\gamma_0 \propto \frac{C_1\sqrt{s}\mu}{m} \qquad \gamma_1 \propto \frac{C_1\sqrt{s}}{m}\frac{\partial\mu}{\partial H|_0}$$

$$\gamma_2 \propto \frac{C_1\sqrt{s}}{2m}\frac{\partial^2\mu}{\partial H^2|_0}$$

where μ is the shear modulus and C_1 is a non-dimensional constant depending on the shape of the projectile. Therefore, γ_0 is directly proportional to μ and characterizes the shear resistance of sand. Hence γ_0 was called here a resistance coefficient. When μ is equal to zero, as in water, γ_0, γ_1 and γ_2 are equal to zero as well. Hence, the static component F_3 of the resisting force is equal to zero. When the cross sectional area of a projectile, s, and the partial derivatives $\partial\mu/\partial H$ and $\partial^2\mu/\partial H^2$ increase, the static component F_3 increases as well.

Equation (4) allows both qualitative and quantitative analysis of the projectile's penetration. It shows that F consists not only of pure dynamic and static components, but also of a mixed component defined by the term $-\gamma_0\varepsilon\dot{H}^2H$ that was derived for the arbitrary function F by the series expansion (3). As will be shown later, this term is very important for interpretation of experimental results.

At small velocities $\dot{H} \to 0$, $\ddot{H}$ in equation (4) and hence F in (1) are defined only by the static component F_3. Therefore, static and dynamic experiments should give similar results. At relatively high velocities, the contributions of $\beta\dot{H}^2$ and $\gamma_0\varepsilon H\dot{H}^2$ may be significant. Hence, F becomes non-monotonic and different from the static F_3. Therefore, analysis of the non-monotonic functional dependence of F on H is important both theoretically and practically. It allows one to assess the static properties of granular media in terms of the dynamic characteristics of projectile penetration.

Equation (4) should be solved for the following initial conditions:

$$\begin{aligned} H(t=0) &= 0 \\ \dot{H}(t=0) &= v_0. \end{aligned} \tag{5}$$

Then its first integral gives the velocity as a function of depth:

$$\begin{aligned} \dot{H}^2 = {} & \mathrm{e}^{-2\beta H - \epsilon\gamma_0 H^2}\left(2\int_0^H (\delta - \gamma_0 H - \gamma_1 H^2 - \gamma_2 H^3) \right. \\ & \left. \times \mathrm{e}^{2\beta H + \epsilon\gamma_0 H^2}\,\mathrm{d}H + v_0^2\right). \end{aligned} \tag{6}$$

By partial differentiation of (6) with respect to time or substitution of (6) into the original equation (4), the variation of acceleration with depth is derived as

$$\begin{aligned} \ddot{H} = {} & -(\beta + \gamma_0\epsilon H)\mathrm{e}^{-2\beta H - \epsilon\gamma_0 H^2} \\ & \left(2\int_0^H (\delta - \gamma_0 H - \gamma_1 H^2 - \gamma_2 H^3) \right. \\ & \left. \times \mathrm{e}^{2\beta H + \epsilon\gamma_0 H^2}\,\mathrm{d}H + v_0^2\right) + \delta - \gamma_0 H - \gamma_1 H^2 - \gamma_2 H^3. \end{aligned} \tag{7}$$

The maximum depth of the projectile's penetration H_m is attained when the velocity $\dot{H}^2$ derived in (6) is equal to zero:

$$\dot{H}^2 = 2\int_0^{H_m} (\delta - \gamma_0 H - \gamma_1 H^2 - \gamma_2 H^3) \times e^{2\beta H + \epsilon\gamma_0 H^2}\, dH + v_0^2 = 0. \quad (8)$$

Equations (7) and (8) show that F at $H = H_m$ should be equal to F_3 and that

$$\ddot{H} = \delta - \gamma_0 H_m - \gamma_1 H_m^2 - \gamma_2 H_m^3. \quad (9)$$

Analysis of equations (6)–(8) is performed here for two extreme cases. The first one corresponds to initial impact velocities less than 10 m s^{-1} and loose sand and is represented by the conditions $\epsilon = 0$ and $\gamma_2 = 0$. After substitution of these zero values in equation (6), the obtained integral has an analytical solution. In a similar manner, equations (11) and (12) are derived from equations (7) and (8):

$$\dot{H}^2 = \left(v_0^2 - \frac{\delta}{\beta} - \frac{\gamma_0}{2\beta^2} + \frac{\gamma_1}{2\beta^3}\right) e^{-2\beta H} + \left(\frac{\gamma_1}{\beta^2} - \frac{\gamma_0}{\beta}\right) H - \frac{\gamma_1 H^2}{\beta} + \frac{\delta}{\beta} + \frac{\gamma_0}{2\beta^2} - \frac{\gamma_1}{2\beta^3} \quad (10)$$

$$\ddot{H} = -\beta\left(v_0^2 - \frac{\delta}{\beta} - \frac{\gamma_0}{2\beta^2} + \frac{\gamma_1}{2\beta^3}\right) e^{-2\beta H} + \frac{\gamma_1}{2\beta^2} - \frac{\gamma_0}{2\beta} - \frac{\gamma_1}{\beta} H \quad (11)$$

$$\left(v_0^2 - \frac{\delta}{\beta} - \frac{\gamma_0}{2\beta^2} + \frac{\gamma_1}{2\beta^3}\right) e^{-2\beta H_m} + \left(\frac{\gamma_1}{\beta^2} - \frac{\gamma_0}{\beta}\right) \times H_m - \frac{\gamma_1 H_m^2}{\beta} + \frac{\delta}{\beta} + \frac{\gamma_0}{2\beta^2} - \frac{\gamma_1}{2\beta^3} = 0. \quad (12)$$

Equation (12) defines the maximum depth of the projectile's penetration in terms of its dependence on the initial velocity v_0 and the static properties of the sand γ_0, γ_1 and β. After substitution of $H_m(v_0)$ into equation (11), we obtain $\ddot{H}(v_0)$ when the projectile stops. In the general case, this should be done graphically.

A thin and heavy projectile penetrating loose sand creates the additional condition $\beta = 0$. The analytical solution of equation (12) for $\gamma_1 = 0$ is achieved by expanding $e^{-2\beta H_m}$ to the second-order terms, then rearranging (12) eliminating the terms equal to zero:

$$H_m \approx \frac{\delta}{\gamma_0} + \sqrt{\left(\frac{\delta^2}{\gamma_0^2} + \frac{v_0^2}{\gamma_0}\right)}. \quad (13)$$

For $v_0 \gg \delta/\sqrt{\gamma_0}$, H_m becomes approximately equal to $v_0/\sqrt{\gamma_0}$. This value of H_m is then substituted into equation (9) to derive the acceleration

$$\ddot{H} \approx -v_0\sqrt{\gamma_0} \quad (13)$$

under the same approximations. Now it is possible to derive the depth of penetration H_e when $\dot{H}$ is at its maximum. After differentiation of (10) with respect to H, the derived expression is equal to 0 at H_e and hence

$$2\beta\left(-v_0^2 + \frac{\delta}{\beta} + \frac{\gamma_0}{2\beta^2} - \frac{\gamma_1}{2\beta^3}\right) e^{-2\beta H_e} = 2\frac{\gamma_1}{\beta} H_e + \frac{\gamma_0}{\beta} - \frac{\gamma_1}{\beta^2}. \quad (14)$$

After taking natural logarithms of both sides (14)

$$H_e = -\frac{1}{2\beta} \ln\left(\frac{\beta\gamma_0[1 + \gamma_1(2\beta H_e - 1)/(\beta\gamma_0)]}{2\beta^2[\delta + (\gamma_0/2\beta)(1 - \gamma_1/\beta\gamma_0) - \beta v_0^2]}\right) \quad (15)$$

For $\gamma_1 = 0$ equation (15) becomes

$$H_e \approx -\frac{1}{2\beta} \ln\left(\frac{\gamma_0}{2\beta^2\left(\frac{\gamma_0}{2\beta^2} + \frac{\delta}{\beta} - v_0^2\right)}\right). \quad (15')$$

Equation (15′) is approximately true for $|\gamma_1(2\beta H_e - 1)|/(\beta\gamma_0) \ll 1$ with $|\gamma_1|/(\beta\gamma_0) \ll 1$ as well. This shows that the maximum $\dot{H}(H)$ will be observed when $v_0 < (\delta/\beta)^{1/2}$. With increasing v_0, H_e becomes smaller, $H_e = 0$ at $v_0 = (\delta/\beta)^{1/2}$ and at $v_0 > (\delta/\beta)^{1/2}$ there is no maximum of H_e defined by equation (10).

$\ddot{H}(H)$ defined by equation (11) may have a maximum when $\gamma_1 < 0$. After taking the derivative of (11) with respect to H and putting it equal to 0, the maximum $\ddot{H}$ will be observed at depth H_d:

$$H_d = -\frac{1}{2\beta} \ln\left(\frac{|\gamma_1|}{2\beta^2\delta + \beta\gamma_0 + |\gamma_1| - 2\beta^3 v_0^2}\right) \quad (16)$$

which is defined for $2\beta^2\delta + \beta\gamma_0 - 2\beta^3 v_0^2 > 0$. The acceleration of a projectile at H_d is

$$\ddot{H} = -\frac{\gamma_0}{2\beta} - \frac{|\gamma_1|}{2\beta^2} \ln\left(\frac{|\gamma_1|}{2\beta^2\delta + \beta\gamma_0 + |\gamma_1| - 2\beta^3 v_0^2}\right). \quad (17)$$

Now we have the second extreme case, in which $\beta = 0$ and $\epsilon \neq 0$. Integration by parts of (6), (7) and (8) gives respectively

$$\dot{H}^2 = e^{-\gamma_0\epsilon H^2}\left[\left(\frac{\gamma_1}{\gamma_0\epsilon} + 2\delta\right)\int_0^H e^{\gamma_0\epsilon H^2}\, dH + \frac{1}{\epsilon}(1 - e^{\gamma_0\epsilon H^2}) - \frac{\gamma_1 H}{\gamma_0\epsilon} e^{\gamma_0\epsilon H^2} + \frac{\gamma_2}{(\gamma_0\epsilon)^2}[(1 - \gamma_0\epsilon H^2)e^{\gamma_0\epsilon H^2} - 1] + v_0^2\right] \quad (18)$$

$$\ddot{H} = -\epsilon\gamma_0 H e^{-\gamma_0\epsilon H^2}\left[\left(\frac{\gamma_1}{\gamma_0\epsilon} + 2\delta\right)\int_0^H e^{\gamma_0\epsilon H^2}\, dH + \frac{1}{\epsilon}(1 - e^{\gamma_0\epsilon H^2}) - \frac{\gamma_1 H}{\gamma_0\epsilon} e^{\gamma_0\epsilon H^2} + \frac{\gamma_2}{(\gamma_0\epsilon)^2}[(1 - \gamma_0\epsilon H^2) \times e^{\gamma_0\epsilon H^2} - 1] + v_0^2\right] + \delta - \gamma_0 H - \gamma_1 H^2 - \gamma_2 H^3 \quad (19)$$

$$\left(\frac{\gamma_1}{\gamma_0\epsilon} + 2\delta\right)\int_0^{H_m} e^{\gamma_0\epsilon H^2}\, dH + \frac{1}{\epsilon}(1 - e^{\gamma_0\epsilon H^2}) - \frac{\gamma_1 H_m}{\gamma_0\epsilon} e^{\gamma_0\epsilon H_m^2} + \frac{\gamma_2}{(\gamma_0\epsilon)^2}[(1 - \gamma_0\epsilon H_m^2)e^{\gamma_0\epsilon H_m^2} - 1] + v_0^2 = 0. \quad (20)$$

Equations (18)–(20) are still too complicated for non-numerical analysis. The integral $\int_0^H e^{\gamma_0\epsilon H^2}\, dH$ cannot be solved analytically, but it is possible to show numerically that its contributions to $\dot{H}$ and $\ddot{H}$ are small. For qualitative assessment of the problem, let us assume the case in which $\gamma_1 = -2\delta\gamma_0\varepsilon$. That permits us to perform analytical integration. Then equations (19) and (20) become

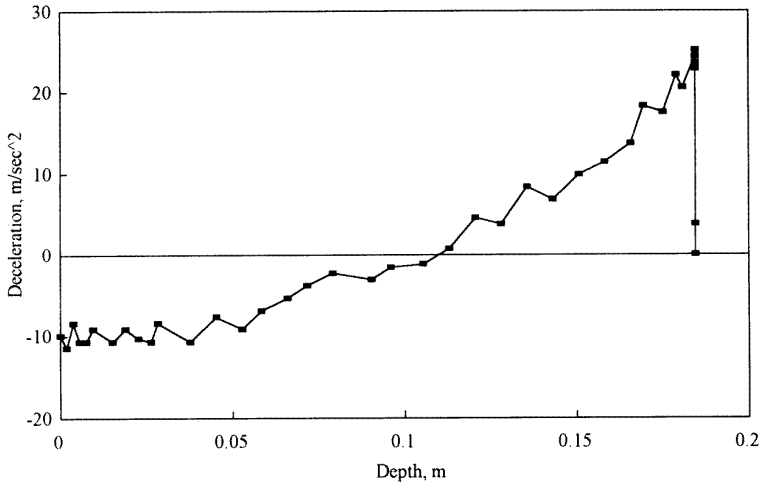

Figure 2. Penetrometer deceleration for v_0 = 0 m s^{-1} in sand of minimum density in an atmospheric test.

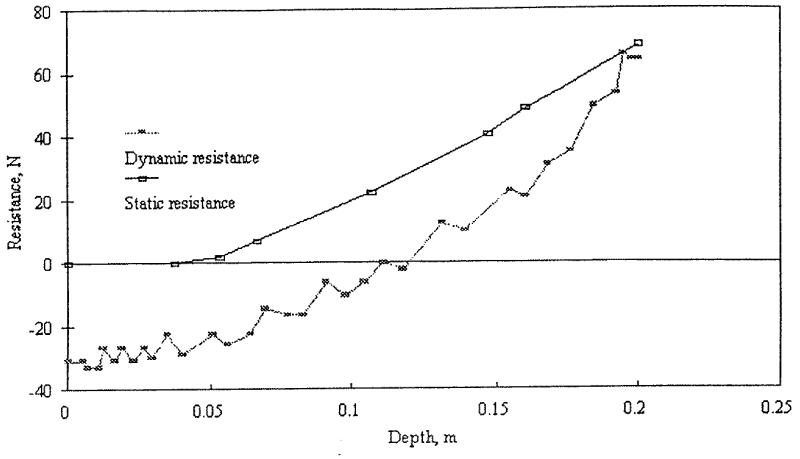

Figure 3. The static and dynamic resistance to penetration at v_0 = 0.0 m s^{-1} in sand of minimum density in atmospheric tests.

$$\ddot{H} = \delta - \gamma_0 H(1+\epsilon v_0^2) \times e^{-\epsilon\gamma_0 H^2} - \frac{\gamma_2}{\gamma_0\epsilon} H(1-e^{-\epsilon\gamma_0 H^2}) \tag{21}$$

$$1 - e^{\gamma_0\epsilon H_m^2} - \frac{\gamma_1 H_m}{\gamma_0} e^{\gamma_0\epsilon H_m^2} + \frac{\gamma_2}{\gamma_0^2\epsilon}[(1-\gamma_0\epsilon H_m^2) \times e^{\gamma_0\epsilon H_m^2} - 1] + \epsilon v_0^2 = 0. \tag{22}$$

Equation (22) defines how H_m depends on v_0 for given γ_0, ε, γ_1 and γ_2 and may be solved graphically. By substituting this solution in (9), $\ddot{H}$ as a function of v_0 at the moment of the projectile stopping is derived.

For $\gamma_2 \approx 0$ and $\gamma_1 H_m/\gamma_0 \ll 1$, the solution of (22) is

$$H_m = -\frac{\gamma_1}{2\gamma_0^2\epsilon} + \left(\frac{\gamma_1^2}{4\gamma_0^4\epsilon^2} + \frac{1}{\gamma_0\epsilon}\ln(1+\epsilon v_0^2)\right)^{1/2}. \tag{23}$$

Let us determine the depths H_i at which extreme values of $\ddot{H}$ are observed. To achieve this, equation (21) is differentiated with respect to H and put equal to 0:

$$\gamma_0(1+\epsilon v_0^2)e^{-\epsilon\gamma_0 H_i^2} - 2H_i^2[\gamma_0^2\epsilon(1+\epsilon v_0^2) - \gamma_2]e^{-\gamma_0\epsilon H_i^2} + \frac{\gamma_2}{\gamma_0\epsilon}(1-e^{-\epsilon\gamma_0 H_i^2}) = 0. \tag{24}$$

For $\gamma_2 = 0$, from (24) it follows that

$$H_1 = \frac{1}{(2\gamma_0\epsilon)^{1/2}} \tag{25}$$

at which $-\ddot{H}$ has the maximum defined in equation (21):

$$-\ddot{H}_m = -\delta + \left(\frac{\gamma_0}{2\epsilon}\right)^{1/2}(1+\epsilon v_0^2)e^{-0.5}. \tag{26}$$

This maximum of acceleration is observed in experiments for relatively large values of v_0, γ_0 and ε.

For $\gamma_2 > 0$, equation (24) may have two solutions H_1 and H_2, where H_1 defines the maximum $-\ddot{H}_m$ and $H_2 > H_1$ corresponds to the minimum $-\ddot{H}_{min}$. Therefore, two peaks of acceleration are observed: the initial and the final peaks as in figure 1(*b*). The initial peak has a dynamic origin and the final peak has a static origin.

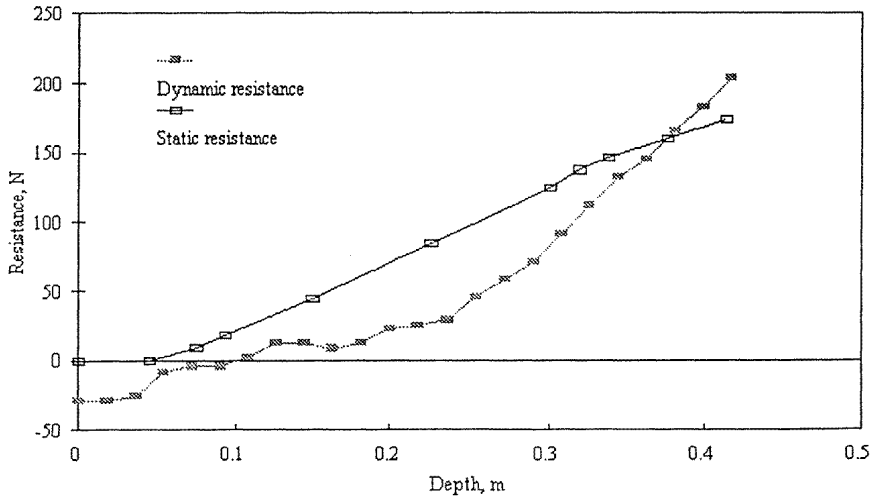

Figure 4. The static and dynamic resistance to penetration at v_0 = 4.1 m s^{-1} in sand of minimum density in atmospheric tests.

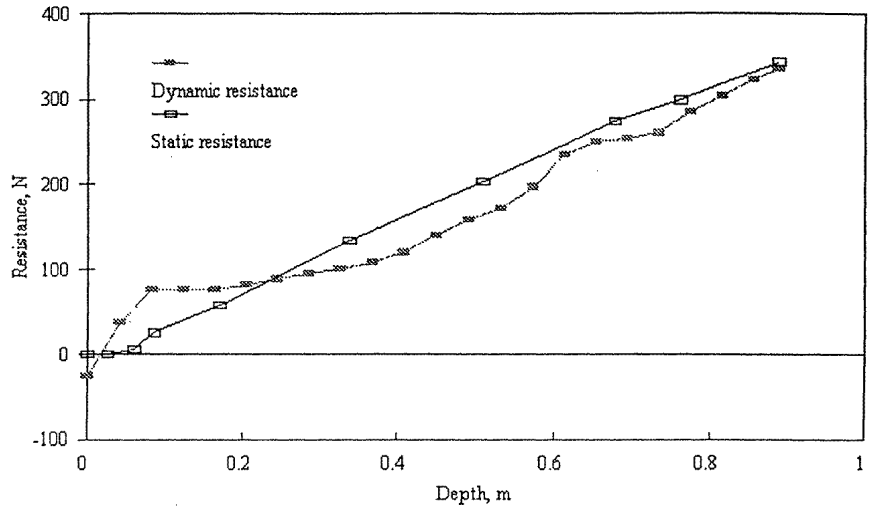

Figure 5. The static and dynamic resistance to penetration at v_0 = 10 m s^{-1} in sand of minimum density in atmospheric tests.

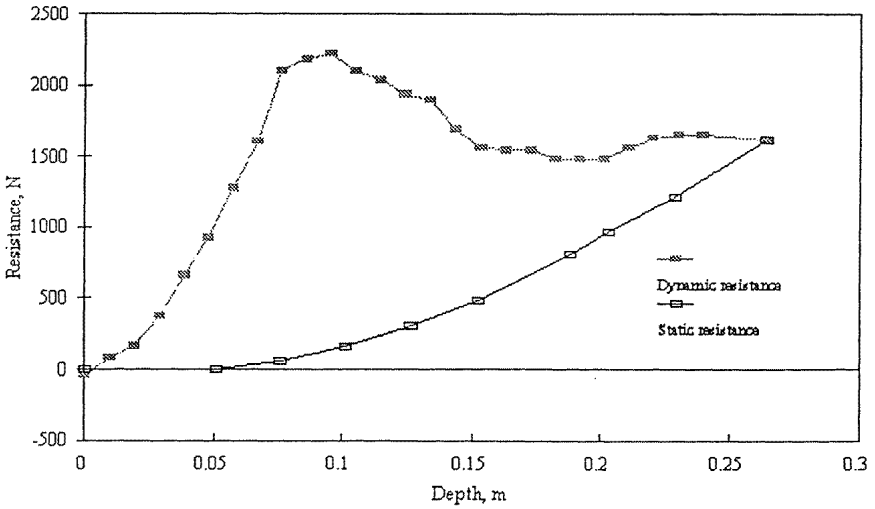

Figure 6. The static and dynamic resistance to penetration at v_0 = 19.2 m s^{-1} in sand of maximum density in vacuum tests.

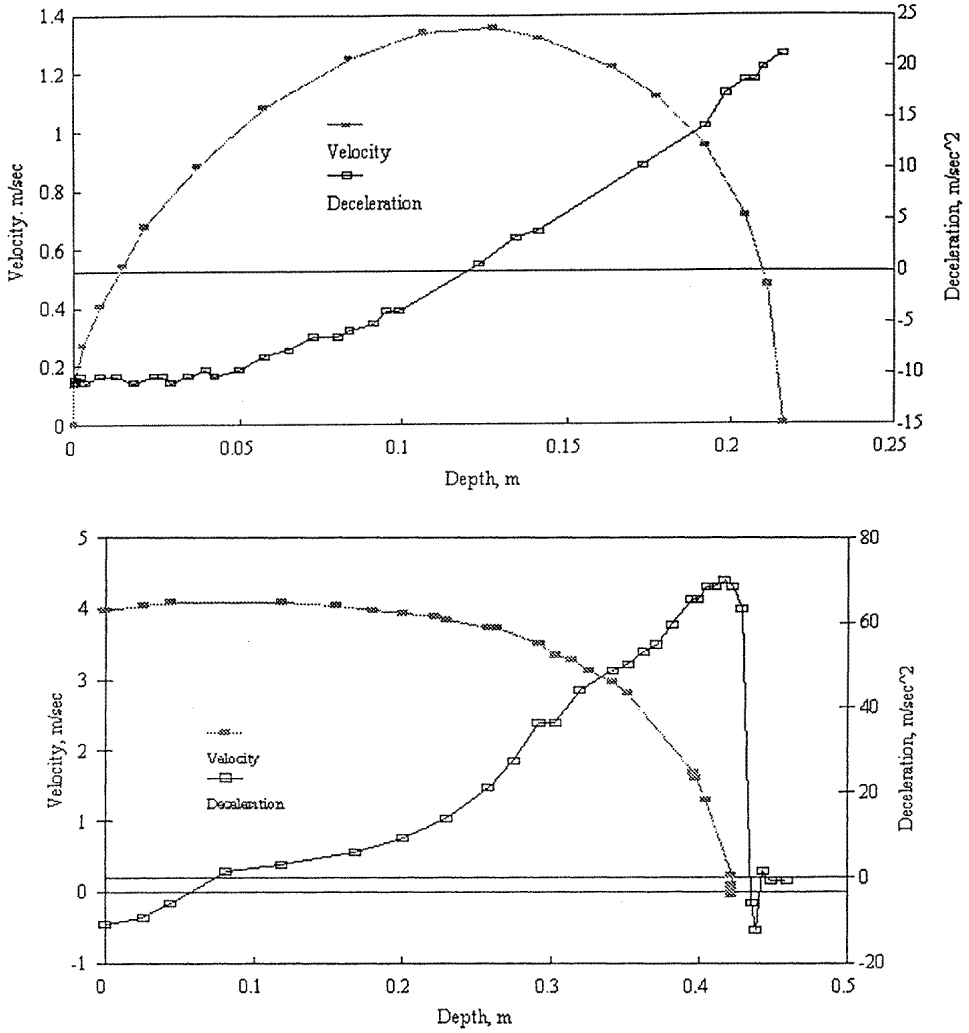

Figure 7. Penetrometer deceleration and velocity in sand of minimum density in vacuum test, for (*a*) $v_0 = 0.0$ m s^{-1} and (*b*) $v_0 = 4.05$ m s^{-1}.

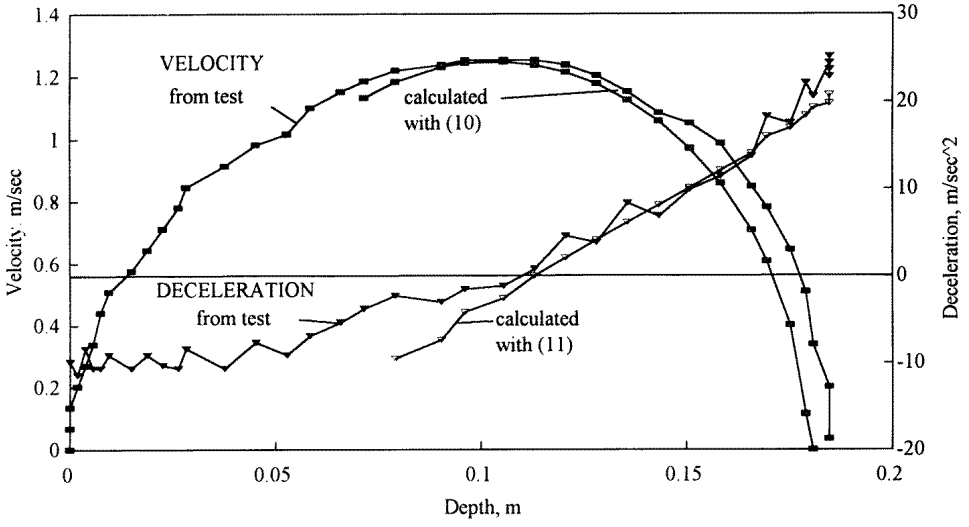

Figure 8. Penetrometer deceleration and velocity for $v_0 = 0.0$ m s^{-1} in sand of minimum density in an atmospheric test.

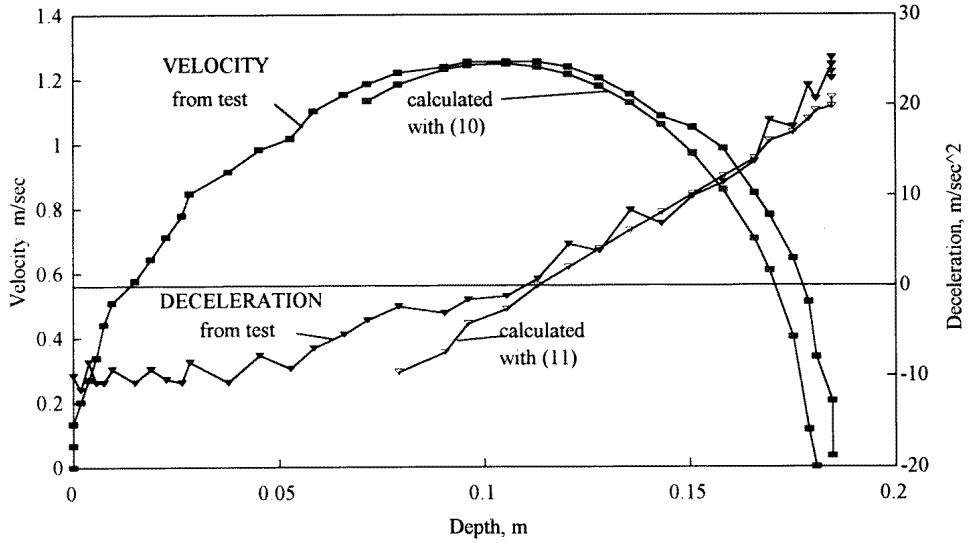

Figure 9. Penetrometer deceleration and velocity for v_0 = 0.0 m s^{-1} in sand of maximum density in an atmospheric test.

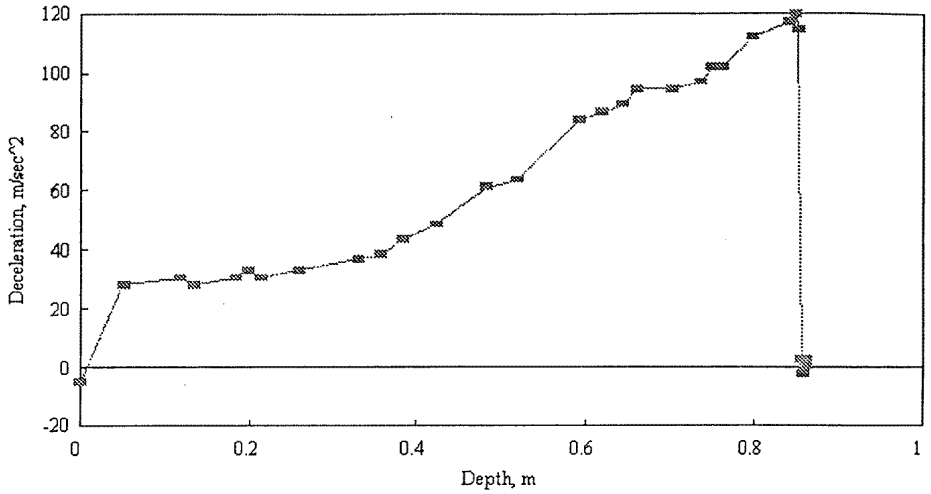

Figure 10. The penetrometer deceleration for v_0 = 10 m s^{-1} in sand of minimum density in a vacuum test.

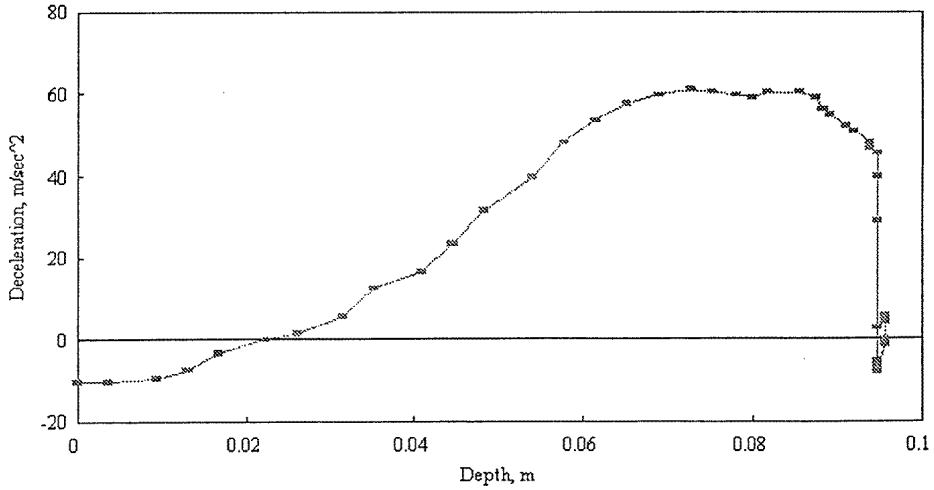

Figure 11. The penetrometer deceleration for v_0 = 2.3 m s^{-1} in sand of maximum density in an atmospheric test.

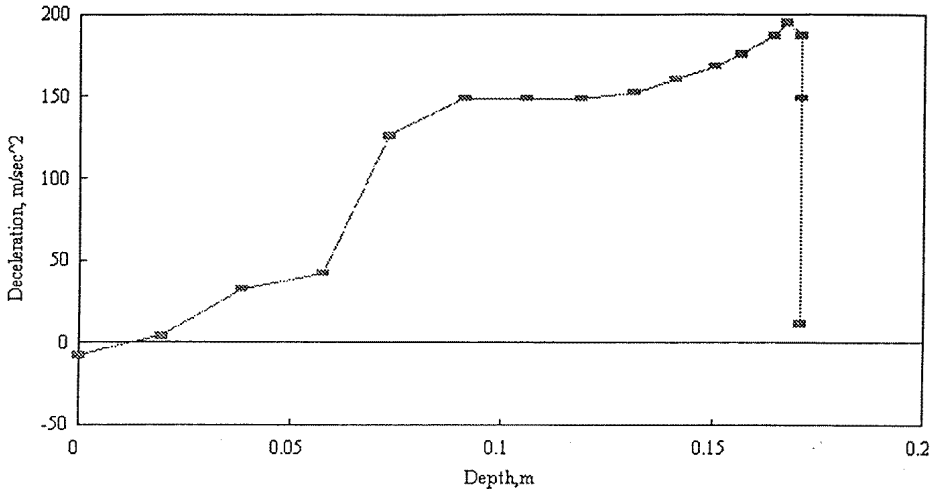

Figure 12. The penetrometer deceleration for v_0 = 6.1 m s^{-1} in sand of maximum density in an atmospheric test.

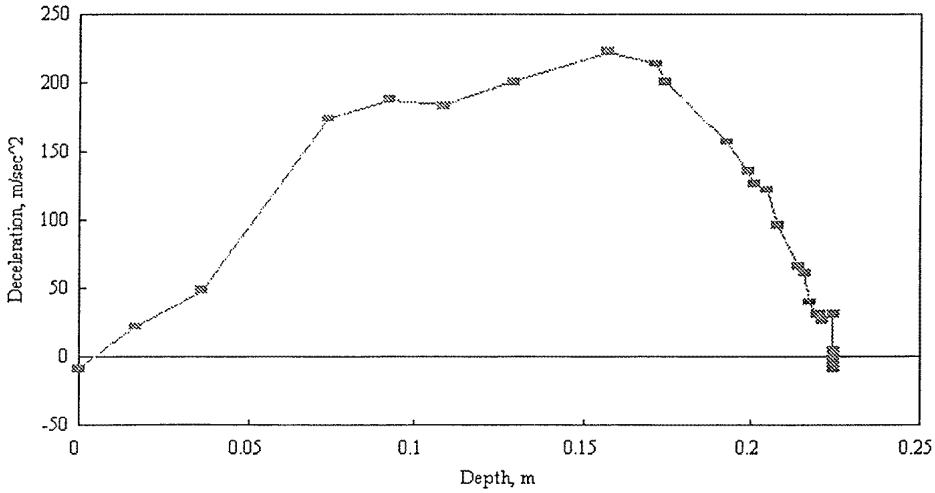

Figure 13. The penetrometer deceleration for v_0 = 8.2 m s^{-1} in sand of maximum density in a vacuum test.

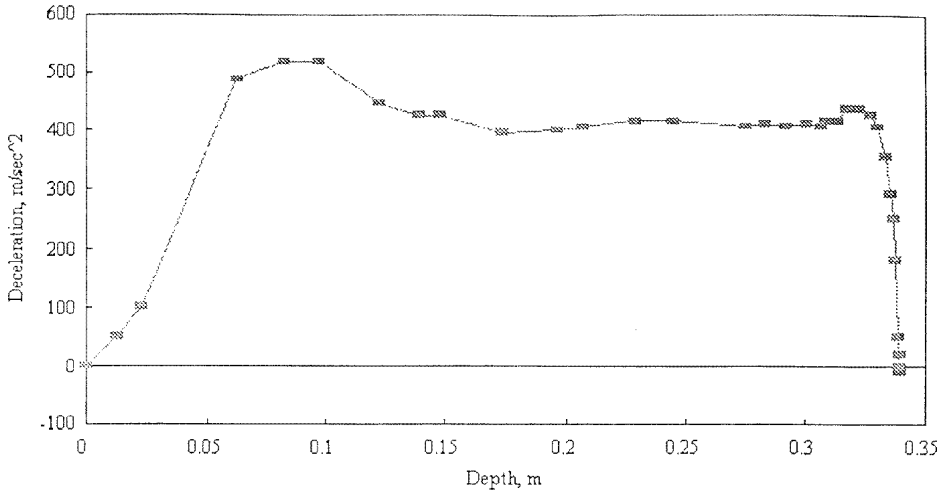

Figure 14. The penetrometer deceleration for v_0 = 15.6 m s^{-1} in sand of maximum density in a vacuum test.

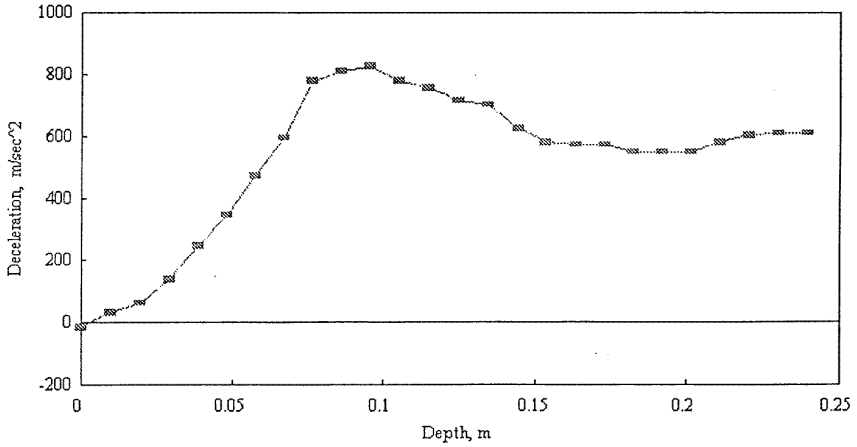

Figure 15. The penetrometer for v_0 = 19.2 m s^{-1} in sand of maximum density in a vacuum test.

4. A comparison between the theoretical model and experimental data

Thompson (1975) presented experimental data using various British units. The original data have been converted into SI units. Typical variations of $\ddot{H}$ with depth are shown in figure 1(b) for $v_0 = 16$ m s^{-1} in sand of medium density tested in vacuum. The plot exhibits dynamic and static peaks of acceleration. Only a static deceleration peak is present in figure 2 for $v_0 = 0$ m s^{-1} in sand of minimum density. The appearance of one or two peaks is related to a combination of v_0 and sand properties, as was predicted in equation (24).

The static properties of sand at different depths may be assessed by using dynamic penetration tests, as follows. The suggested model showed that dynamic and static resistance forces differ substantially for large velocities of a projectile in sand. From equation (8), these forces are similar at the depth H_m when the projectile stops. This conclusion is a general one, which does not depend on the formulation of equation (4).

Figures 3–5 demonstrate examples of the evolution of dynamic and static resistance with respect to H in loose sand at $v_0 = 0.0$, 4.1 and 10 m s^{-1}. Figure 6 shows the same for dense sand at $v_0 = 19.2$ m s^{-1}. Figures 3–6 show that, when the projectile stops, there is close matching of the static and dynamic resistances: 65 and 67, 160 and 210, 310 and 320 and 1620 and 1680 N, respectively. Therefore, the static resistance of sand at depth H_m can be evaluated by measuring the projectile's acceleration. By varying v_0, sand resistance can be assessed at different depths.

The value of β may be derived from (4′) when coefficient C is determined for a projectile of a given shape. Otherwise C may be assessed from the following considerations. When $v_0 = 0$ m s^{-1}, a maximum velocity exists at a certain depth $H \neq 0$, as shown in figure 7(a). When v_0 increases, the location of that maximum moves towards $H \approx 0$ (figure 7(b)). At $H_e = 0$ in (15), β is about δ/v_0^2, where δ is the acceleration at $H = 0$. From figure 7(b), δ is about 10 m s^{-2} and $\beta \approx 0.6$ m^{-1}. From experimental data, γ_0 may be derived from equation (15′) when β is known.

In this paper, $\gamma_0 = 190$ s^{-2} was derived for sand of minimum density in vacuum (figure 7(a)). Under atmospheric pressure, the same sand was characterized by higher γ_0 of 275 s^{-2} (figure 8) and sand of maximum density sand had $\gamma_0 = 650$ s^{-2} (figure 9). Note that increasing the confining pressure (presence of atmospheric pressure) and/or small variations in sand density caused a substantial increase in the resistance coefficient. From conventional static tests, similar variations of μ were found in other studies (Morland 1992, Tatsuoka *et al* 1994, Drabkin 1995).

Equation (11) allows one to evaluate the acceleration when the projectile stops, assuming that $\gamma_1 = 0$. In vacuum tests, sand of minimum density had $\gamma_0 = 190$ s^{-2} and for $v_0 = 10$ m s^{-1} the last peak of acceleration is $-\ddot{H} \approx 138$ m s^{-2}, which matches well with $-\ddot{H} \approx 120$ m s^{-2} in figure 10. In atmospheric tests, sand of maximum density had $\gamma_0 = 650$ s^{-2}; for $v_0 = 2.3$ and 6.1 m s^{-1}, $-\ddot{H} \approx 57$ and 156 m s^{-2}, respectively, which also matches the experimental values $-\ddot{H} \approx 60$ and 180 m s^{-2} in figures 11 and 12.

With increasing v_0 and sand density, the term $\gamma_0 \varepsilon H \dot{H}^2$ in equation (4) may become the dominant one. Hence an initial dynamic acceleration peak will be observed. Equation (26) allows one to estimate this peak's value.

The value of ϵ may be derived from equation (25). It does not depend on v_0. For example, at maximum deceleration, the depth H_1 is about 0.15 m (figure 13). Hence, $\epsilon = 0.08$ s^2 m^{-2}. For $v_0 = 8.2$, 15.6 and 19.2 m s^{-1}, the first dynamic acceleration peak calculated from equation (26) has values of 231, 759 and 1135 m s^{-2}. From figures 13–15, the experimental values of the peaks are 195, 540 and 850 m s^{-2}, respectively. That is a good matching considering all the approximations used. Oscillations of acceleration observed in experiments are caused by small variations in sand density and will be discussed in a separate paper.

5. Conclusions

(i) The projectile's deceleration in non-dissipative media is characterized by an equation developed from general physical considerations. This equation is analysed for different combinations of parameters.

(ii) The derived solutions define the dependence of projectile velocity and deceleration on its initial impact velocity, time, depth of penetration and the target characteristics.

(iii) The suggested model allows one to explain the observed nonlinear and non-monotonic characteristics of deceleration for various test conditions.

(iv) Static and dynamic sand resistance was investigated for different sand densities and projectile velocities in vacuum and in atmospheric tests. Good agreement exists between the suggested theoretical model and the experiments. Therefore, the various limitations placed upon the values of parameters in the derivation of the equations employed are reasonable.

(v) The static strength of sand may be derived only at the moment when the movement of a projectile stops.

Appendix 1. Analysis of equation (4) for the case of weak nonlinearity

The main body of the paper studies the velocity $\dot{H}$ and deceleration $\ddot{H}$ as functions of depth H. Generally, it is impossible to evaluate analytically H, $\dot{H}$ and $\ddot{H}$ as functions of time t because the differential equation (4) is nonlinear. An exception is the case of weak nonlinearity. Investigation of $H(t)$, $\dot{H}(t)$ and $\ddot{H}(t)$ for two such cases, when $\epsilon = 0$ and $\gamma_2 = 0$, and when $\beta = 0$ and $\gamma_1 = \gamma_2 = 0$, is the goal of this appendix.

For $\epsilon = 0$ and $\gamma_2 = 0$, the suggested model of penetration expressed by equation (4) becomes

$$\ddot{H} + \gamma_0 H = -\beta \dot{H}^2 - \gamma_1 H^2 + \delta. \tag{27}$$

The solution of (27) is found here using the method of successive approximations:

$$H = H^{(1)} + H^{(2)} + H^{(3)}. \tag{28}$$

We start with $H^{(1)}$ that may be expressed as

$$H^{(1)} = \frac{\delta}{\gamma_0} + a\cos(\omega t + \theta) \tag{29}$$

where exact values of frequencies ω need to be found as a series:

$$\omega = \sqrt{\gamma_0} + \omega^{(1)} + \omega^{(2)}. \tag{30}$$

The method of successive approximations requires that periodic terms in the solution contain exact values of frequencies. Variations in frequencies are determined from the solutions of equations using the condition of the absence of resonant terms, as shown by Landau (1961). Now equation (27) may be re-written as

$$\frac{\gamma_0}{\omega^2}\ddot{H} + \gamma_0 H = -\beta \dot{H}^2 - \gamma_1 H^2 - \left(1 - \frac{\gamma_0}{\omega^2}\right)\ddot{H} + \delta. \tag{31}$$

Assuming here that $H = H^{(1)} + H^{(2)}$ and $\omega = \sqrt{\gamma_0} + \omega^{(1)}$ and neglecting small second-order terms, the equation expressing $H^{(2)}$ becomes

$$\ddot{H}^{(2)} + \gamma_0 H^{(2)} = -A + \tfrac{1}{2}a^2(\beta\gamma_0 - \gamma_1)\cos[2(\omega t + \theta)] \tag{32}$$

where

$$A = \beta\frac{a^2\gamma_0}{2} + \gamma_1\frac{\delta^2}{\gamma_0^2} + \frac{1}{2}a^2\gamma_1.$$

In this equation the condition of the absence of resonant terms gives

$$\omega^{(1)} = \frac{\gamma_1\delta}{\gamma_0\sqrt{\gamma_0}}.$$

The solution of (32) is

$$H^{(2)} = -\frac{A}{\gamma_0} - \frac{a^2(\beta\gamma_0 - \gamma_1)}{6\gamma_0}\cos[2(\omega t + \theta)]. \tag{33}$$

Then, assuming in (31) $H = H^{(1)} + H^{(2)} + H^{(3)}$ and $\omega = \sqrt{\gamma_0} + \omega^{(1)} + \omega^{(2)}$ and taking into account (29) and (33), the condition of there being a resonant term gives

$$\omega^{(2)} = \beta B\sqrt{\gamma_0} + \frac{\gamma_1 B}{2\sqrt{\gamma_0}} - \gamma_1\frac{A}{\gamma_0\sqrt{\gamma_0}}$$

where

$$B = \frac{a^2(\gamma_1 - \beta\gamma_0)}{6\gamma_0}.$$

The equation for $H^{(3)}$ becomes

$$\ddot{H}^{(3)} + \gamma_0 H^{(3)} = B\left(8\sqrt{\gamma_0}\omega_1 - 2\gamma_1\frac{\delta}{\gamma_0}\right)\cos[2(\omega t + \theta)] + Ba(2\beta\gamma_0 - \gamma_1)\cos[3(\omega t + \theta)] + 2\gamma_1\frac{\delta A}{\gamma_0^2}. \tag{34}$$

The solution to third order is

$$H^{(3)} = -\frac{N}{3\gamma_0}\cos[2(\omega t + \theta)] - \frac{M}{8\gamma_0}\cos[3(\omega t + \theta)] + 2\gamma_1\frac{\delta A}{\gamma_0^3} \tag{35}$$

where

$$N = 8\sqrt{\gamma_0}\omega^{(1)} - 2\gamma_1\frac{\delta}{\gamma_0} \qquad M = Ba(2\beta\gamma_0 - \gamma_1).$$

Now we analyse equation (4) when $\beta = 0$ and $\gamma_1 = \gamma_2 = 0$:

$$\ddot{H} + \gamma_0 H = -\epsilon\gamma_0\dot{H}^2 H + \delta. \tag{36}$$

The solution of this equation is derived using the Krylov–Bogoliubov technique (Nayfeh 1973) for small $\varepsilon_1 = \varepsilon\gamma_0 H_m^2 \ll 1$. The first-order solution may be presented as

$$H = H_m a\cos\psi + H_m\epsilon_1 u_1(t) + \frac{\delta}{\gamma_0}. \tag{37}$$

The value of H_m is derived from (20) considering $\gamma_1 = \gamma_2 = 0$. On substituting (37) into (36) and skipping terms that generate resonant terms, ψ and u_1 are derived as follows:

$$\psi = \sqrt{\gamma_0}\left(1 + \frac{\epsilon_1 a^2}{8}\right)t + \theta \tag{38}$$

$$\frac{\mathrm{d}^2 u_1}{\mathrm{d}t^2} + \gamma_0 u_1 = -\frac{\delta a^2}{H_m}[1 - \cos(2\psi)] + \frac{\gamma_0 a^3}{4}\cos(3\psi) \tag{39}$$

where the solution of (39) is

$$u_1 = -\frac{\delta a^2}{\gamma_0 H_m} - \frac{\delta a^2}{3\gamma_0 H_m}\cos(2\psi) - \frac{a^3}{32}\cos(3\psi). \qquad (40)$$

The values of constants a and θ are derived from the initial conditions (5). The second-order solution is negligible.

References

Allen W A *et al* 1957 Dynamics of a projectile penetrating sand *J. Appl. Phys.* **28**

Drabkin S 1995 Low level vibration induced settlement of granular soils *PhD Dissertation* Polytechnic University, Brooklyn, New York

Euler L 1745 *Neue Grundsätze der Artillerie* Berlin (Reprinted *Euler's Opera Omnia* vol 14, series II (Teubner))

Forrestal M J, Brar N S and Luk V K 1991 Penetration of strain-hardening targets with rigid spherical-nose rods *ASME J. Appl. Mech.* **58** 7–10

Forrestal M J, Lee L M and Jenrette L M 1986 Laboratory-scale penetration experiments into geological targets to impact velocities of 2.1 km/s *ASME J. Appl. Mech.* **53** 317–20

Hearst J R and Lynch C S 1994 Measurement of *in situ* strength using projectile penetration *Int. J. Rock Mech., Mining Sci. Geomech. Abstracts* **31** 243–51

Jaeger H M and Nagel S R 1992 Physics of the granular state *Science* March 1523–31

Korn G A and Korn T M 1968 *Mathematical Handbook* (New York: McGraw-Hill)

Landau L D and Lifshitz E M 1959 *Mechanics* (New York: Pergamon)

Morland L W 1992 Compaction and shear settlement of granular materials *J. Mech. Phys. Solids* **41** 507–30

Nayfeh A H 1973 *Perturbation Methods* (New York: Wiley)

Rachmatullin Kh A, Sogomonyan A Ya, Alekseev A A 1964 *Soil Dynamics* (Moscow) (in Russian)

Robins B 1742 *New Principles of Gunnery* (London: Nourse)

Sedov L I 1959 *Similarity and Dimensional Methods in Mechanics* (New York: Academic)

Sogomonyan A Ya 1974 *The Theory of Penetration Phenomena J. Mech. Solids*

Tatsuoka F *et al* 1994 Measurements of elastic properties of geomaterials in laboratory compression tests *Geotech. Testing J.* **17** 80–94

Taylor T, Fragaszy R J and Ho C L 1991 Projectile penetration in granular soils *ASCE J. Geotech. Eng.* **117** 658–72

Thompson J B III 1975 Low-velocity impact penetration of low-cohesion soil deposits *Dissertation for the Degree of Doctor of Philosophy in Engineering* University of California, Berkeley

True D G 1976 Undrained vertical penetration into ocean bottom soils *Dissertation for the Degree of Doctor of Philosophy in Engineering* University of California, Berkeley

Zukas J A, Nicholas T, Swift H F, Greszczuk L and Curra D R 1982 *Impact Dynamics* (New York: Wiley)